Flow Mechanisms, Relative Permeabilities, and Coupling Effects in Steady-State Two-Phase Flow through Porous Media. The Case of Strong Wettability

ARTICLE *in* INDUSTRIAL & ENGINEERING CHEMISTRY RESEARCH · JANUARY 1999

Impact Factor: 2.59 · DOI: 10.1021/ie980404o

2 AUTHORS, INCLUDING:

D.G. Avraam

Region of Central Macedonia, Regional Unity …

31 PUBLICATIONS **529** CITATIONS

SEE PROFILE

Flow Mechanisms, Relative Permeabilities, and Coupling Effects in Steady-State Two-Phase Flow through Porous Media. The Case of Strong Wettability

D. G. Avraam and A. C. Payatakes*

Department of Chemical Engineering, University of Patras and Institute of Chemical Engineering and High-Temperature Chemical Processes, P.O. Box 1414, GR 265 00 Patras, Greece

The pore-scale flow mechanisms and the relative permeabilities during steady-state two-phase flow in a glass model pore network were studied experimentally for the case of strong wettability ($\theta_e < 10°$). The capillary number, the fluid flow rate ratio, and the viscosity ratio were changed systematically, while all other parameters were kept constant. The flow mechanisms at the microscopic and macroscopic scales were examined visually and videorecorded. As in the case of intermediate wettability, we observed that over a broad range of values of the system parameters the pore-scale flow mechanisms include many strongly nonlinear phenomena, specifically, breakup, coalescence, stranding, mobilization, etc. Such microscopically irreversible phenomena cause macroscopic nonlinearity and irreversibility, which make an Onsager-type theory inappropriate for this class of flows. The main effects of strong wettability are that it changes the domains of the system parameter values where the various flow regimes are observed and increases the relative permeability values, whereas the qualitative aspects of the flow remain the same. Currently, a new true-to-mechanism model is being developed for this class of flows.

1. Introduction

Simultaneous two-phase flow through porous media is of great practical interest for many industrial processes such as secondary and tertiary oil recovery, flow in water aquifers, risk assessment in connection with undergroundwater pollution by liquid organic wastes, etc. For the sake of brevity we will use the terms "water" (fluid 1) and "oil" (fluid 2) to refer to the wetting and nonwetting fluids, respectively, with the understanding that they apply to other pairs of immiscible fluids. When the two fluids flow under fully developed steady-state conditions, their average flow rates and saturations remain constant in the spatiotemporal statistical sense. On the other hand, transient flow involves displacement of one fluid by the other, and it is more complex. In both cases, the conventional theoretical analysis relies on the use of the relative permeabilities of the two fluids as the relevant macroscopic momentum transfer coefficients. However, the origin of the concept of relative permeability is in Darcy's law, which is strictly valid only for creeping one-phase flow. Any empirical or semiempirical extension of this law to include two-phase flow can only be based on strong simplifications and assumptions, the validity of which is now under serious challenge.

Such a drastic assumption concerning the nature of steady-state two-phase flow in porous media (SS2φFPM) is that the two fluids flow under their own pressure gradient through bicontinuous pathways, which remain invariant (static).[1] Moreover, it is presumed that when parts of the oil (oil ganglia and droplets) become disconnected from the main oil body, they become immediately trapped within the pore space. This, in turn, implies that completely disconnected oil cannot flow and that under such conditions the relative permeability becomes zero.[2] A direct consequence of this is the prediction that the relation between the macroscopic pressure gradients and the fluid flow rates should be nearly linear and that the proportionality coefficients (relative permeabilities) should be functions of the corresponding fluid saturation only (in addition to the structure of the porous medium). According to this conventional view, the flows of the two fluids are essentially uncoupled, which implies that independent consideration of the pressure gradient and flow rate of each fluid is feasible. As it turns out, these assumptions are seriously wrong.[3,4] A further complication arises from the fact that, in practice, the ultimate objective is to transfer experimental data from steady-state flow to transient two-phase flow (displacement), assuming that the instantaneous, though continuously changing, flow mechanisms in the displacing front of a transient flow are similar at each point and time to those in the corresponding steady-state two-phase flow. As we will see below, such decoupling of the flow is not possible. Under fully developed flow conditions, the two pressure gradients are always identical, whereas small deviations are caused by boundary and end effects.

The aforementioned assumptions have been tested experimentally in a series of works, where we investigated the flow mechanisms and the corresponding relative permeabilities and viscous coupling coefficients during steady-state two-phase flow through *planar* and *nonplanar* glass model porous media.[3−6] The topology of the micromodel is an important factor for all classes of two-phase flow. However, careful experiments conducted on artificial *planar* and *nonplanar* micromodels of the same geometry have shown that the nature of two-phase flow remains *qualitatively* the same and only *quantitative* differences are observed.[5,6] Therefore, in this study we used a large planar micromodel, which is described briefly below, and all experimental data were obtained by using that particular micromodel. In all

* To whom correspondence should be addressed.

10.1021/ie980404o CCC: $18.00
Published on Web 01/27/1999

previous works, we used pairs of immiscible fluids with intermediate wettability ($\theta_e \approx 40°$) with respect to the glass model. Here we extend this study to the case of strong wettability ($\theta_e < 10°$), a factor that favors the formation of wetting films which, in turn, are expected to have strong quantitative (and, conceivably, qualitative) consequences.

The conventional relative permeabilities can be obtained easily from fluid flow rate and pressure drop measurements. The usual precautions concern elimination of boundary and end effects and simultaneous but independent measurement of the pressure drops in each fluid, using semipermeable membranes. It has already been established that the conventional relative permeabilities are nonlinear functions of many system parameters, specifically, capillary number, Ca,[7−10] fluid flow rate ratio, r,[11,12] fluid viscosity ratio, κ,[13,14] equilibrium contact angle, θ_e,[15−17] porous medium characteristics and history of the flow,[17] etc.

Several attempts to obtain a better theoretical model between flow rates and pressure gradients have led to the generalized fractional flow theory. According to this model, the flow rate of each fluid has two contributions, one proportional to the pressure gradient in water and the other to the pressure gradient in oil. The four phenomenological coefficients are called generalized relative permeabilities.[4] In this way, coupling effects between the two flowing fluids are taken into account explicitly. However, this attempt has not succeeded in resolving the complexity of two-phase flow in porous media. The formalism is of the Onsager type, but in reality the nature of the flow is not amenable to such an approach. The generalized fractional flow theory fails on two counts. First, the cross-term coefficients are not equal and, second, the general relative permeability coefficients turn out to be strong functions of the pressure gradient.[4] Thus, an Onsager-type theory seems to be inappropriate for this class of flow phenomena.

An explanation for these observations was proposed recently.[3] The key feature of SS2φFPM is that the flow of oil is effected to a large extent (or in many cases completely) through the motion of disconnected oil, in the form of ganglia and/or droplets. For small values of the capillary number, Ca, the oil is completely disconnected. Oil ganglia and droplets participate in a dynamic process, called ganglion dynamics, which involves motion, entrapment, mobilization, breakup, collision, and coalescence of ganglia and droplets of various sizes and, of course, motion of contact lines. Gradual intensification of the flow (by increasing one or both of the fluid flow rates) leads to the formation of smaller moving ganglia and the appearance of small droplets. Further intensification leads to the formation of connected oil pathways as well as connected water pathways, which however coexist with ganglion dynamics and motion of oil droplets.

Based on the mean size of *moving* ganglia and other relevant flow features, four main flow regimes were distinguished:[3] (1) *large ganglion dynamics (LGD)*, (2) *small ganglion dynamics (SGD)*, (3) *drop traffic flow (DTF)*, and (4) *connected pathway flow (CPF)*. The distinction between large and small moving ganglia is somewhat arbitrary. When the average size of moving ganglia is larger than about 10 chamber volumes, the regime is characterized as LGD; otherwise, it is characterized as SGD. The oil droplets have diameters comparable to those of the throat diameters. An important result is that both conventional and generalized relative permeabilities are strongly correlated with the corresponding flow regimes. Any theoretical model of two-phase flow in porous media should take into account the detailed microscopic flow mechanisms, if it is meant to be true-to-nature.

Table 1. Model Porous Medium Characteristics

	class				
	1	2	3	4	5
chaber diameter D_C (μm)	210	470	610	750	890
throat width D_T (μm)	111	139	169	195	222
frequency	0.16	0.21	0.26	0.21	0.16

cross-sectional area A (m^2)	1.328×10^{-4}
periodicity length l (μm)	1221
mean equvalent capillary diameter d_c (μm)	97.35
mean etching depth w (μm)	116.6
total pore volume V_p (m^3)	7.807×10^{-7}

In what follows, a set of SS2φFPM experiments with a small equilibrium contact angle ($\theta_e < 10°$) is presented. The conventional and generalized relative permeability coefficients are determined as functions of the main system parameters and correlated with the pore-scale mechanisms. The main objectives are to correlate the macroscopic flow behavior with the microscopic flow mechanisms, to clarify the main causes of the nonlinearity of the flow, and to determine the fundamental reasons for which an Osanger-type theory does not apply for this class of flows.

2. Experimental Method and Materials

Details about the experimental porous medium, the apparatus, and the procedure were given in previous publications.[3,4] Here we give a brief description. The model porous medium was constructed by sintering two glass plates with the model pore network etched on their inner surfaces. The pore network was based on a square lattice. On the nodes of the lattice were etched chambers (shaped as circular disks) and on the branches were etched throats (which are cylinders with an "eye-shaped" cross section). The model pore network comprises 11 300 chambers and 22 600 throats. The diameters of the chambers and the widths of the throats were selected from a discrete normal distribution with five classes and with standard deviation equal to $^1/_4$ of the mean value (Table 1). The pore depth, controlled by etching, was 116 ± 20 μm.

The two fluids were injected through the porous medium with syringe pumps through separate inlet ports, with prescribed and virtually constant flow rates, for as long as it was needed to achieve steady-state conditions (typically, 2 h to 2 days). Then, the pressure drops in the two fluids were measured along a central section of the porous medium. The pore-scale mechanisms were continuously monitored and videorecorded. The flow images were analyzed with an image analysis system. All measurements and observations were confined over a central part of the medium that covers ca. $^1/_4$ of the entire model. To ensure that boundary and end effects have been avoided, the central region was partitioned to 12 sections and the oil saturation in each section was determined separately. No statistically significant differences were detected. On the other hand, the equality of (the mean values of) the fluid pressure drops is also an indirect indication that the flow is free from boundary and end effects.

Table 2. Physicochemical Properties of the Pairs of Fluids

Fluid System 1 (Nonwetting Fluid, *n*-Nonanol; Wetting Fluid, Formamide)	
μ_0 (Pa s)	0.00964
μ_w (Pa s)	0.00335
$\kappa = \mu_0/\mu_w$	2.88
ρ_o (kg/m^3)	816
ρ_w (kg/m^3)	1116
γ_{ow} (mN/m)	4.3
θ_e (deg)	9[18]
Fluid System 2 (Nonwetting Fluid, *n*-Dodecane; Wetting Fluid, Deionized Water + 0.34% Extran MA 01 MERCK)	
μ_0 (Pa s)	0.00136
μ_w (Pa s)	0.00087
$\kappa = \mu_0/\mu_w$	1.56
ρ_0 (kg/m^3)	730
ρ_w (kg/m^3)	998
γ_{ow} (mN/m)	9.5
θ_e (deg)	5[19]

3. Fluid System

Two new pairs of fluids were used in the experiments (Table 2). The two pairs were chosen to give strong wettability with respect to glass and viscosity ratios close to those of the pairs of fluids which were used previously[3,4] and which had intermediate wettability. Thus, direct comparison can be made with wettability as the only changing parameter. All other parameters (Ca, r, κ) and the porous medium model were kept constant (or nearly so).

4. Conventional and Generalized Relative Permeabilities

The conventional relative permeabilities are defined by the following expressions:

$$q_i = \frac{k k_{ri}}{\mu_i} A \frac{\Delta P_i}{L}, \quad i = 1, 2 \tag{1}$$

where q_i ($i = 1, 2$) are the flow rates of water and oil, respectively, k is the absolute permeability of the medium, k_{ri} ($i = 1, 2$) are the conventional relative permeabilities, μ_i ($i = 1, 2$) are the viscosities of the fluids, A is the cross-sectional area of the medium, L is the distance along which the pressure drops are measured, and ΔP_i ($i = 1, 2$) are the experimentally measured spatiotemporal average values of the pressure drops of water and oil, respectively.

The generalized relative permeability coefficients, with the viscous coupling effects taken explicitly into account, are defined by the following expressions:

$$q_i = \frac{k k_{rii}}{\mu_i} A \frac{\Delta P_i}{L} + \frac{k k_{rij}}{\mu_j} A \frac{\Delta P_j}{L}, \quad i, j = 1, 2, \quad i \neq j \tag{2}$$

where the diagonal coefficients, k_{rii}, correspond to those parts of the fluid flow rates that can be attributed to pressure drop in the same fluid, whereas the off-diagonal coefficients, k_{rij}, correspond to the remaining parts that are due to the pressure drop in the other fluid and which are attributed to viscous coupling effects.

The aforementioned parameters can be determined from experimental data such as those summarized in Table 3. Thus, we can obtain the conventional and generalized coefficients as functions of the system parameters, specifically,

Table 3. Experimental Data for the Pair of Fluids 1 and 2

r	q_1 (mL/min)	q_2 (mL/min)	S_1 (%)	ΔP_1 (mbar)	ΔP_2 (mbar)	k_{r1} (%)	k_{r2} (%)	χ_1	χ_2
Fluid 1 with $\kappa = 2.88$									
$Ca = 5 \times 10^{-7}$ [a]									
0.47	0.0051	0.0024	55.91	2.89	2.81	7.3364	10.107	0.0014	0.9981
1.16	0.0051	0.0060	47.60	3.27	3.58	6.4909	19.833	0.6811	0.6629
2.33	0.0051	0.0120	33.27	4.17	4.37	5.0791	32.460	0.9996	1.0000
10.70	0.0051	0.0552	18.00	15.16	9.76	1.3984	66.926	0.0000	0.7865
$Ca = 1 \times 10^{-6}$ [b]									
0.25	0.0097	0.0024	63.12	2.58	2.35	15.499	12.087	0.0382	0.7078
0.43	0.0097	0.0042	61.37	3.00	3.67	13.295	13.553	0.1739	0.5905
1.08	0.0097	0.0105	56.28	3.77	4.34	10.577	28.629	0.6020	0.5663
2.47	0.0097	0.0243	51.60	6.67	7.34	5.9883	39.159	1.000	0.6301
10.80	0.0097	0.1050	22.00	16.14	14.05	2.4738	88.394	0.7500	0.6976
$Ca = 5 \times 10^{-6}$ [c]									
0.20	0.0516	0.0105	68.26	7.78	6.55	27.228	18.960	0.1055	0.9999
0.47	0.0516	0.0240	66.10	8.70	9.10	24.366	31.205	0.1167	0.9998
1.07	0.0516	0.0552	58.52	14.83	14.12	14.283	46.257	0.2113	0.9982
2.33	0.0516	0.1200	53.20	22.54	21.42	9.4026	66.287	0.3277	0.9929
10.70	0.0516	0.5520	25.89	118.37	62.63	1.7905	104.27	0.8461	0.8644
Fluid 2 with $\kappa = 1.56$									
$Ca = 5 \times 10^{-7}$ [d]									
0.09	0.0486	0.0042	59.82	12.68	14.36	4.0826	0.4864	1.0000	1.0000
0.57	0.0486	0.0276	27.53	30.90	30.12	1.6758	1.5234	0.3462	1.0000
1.14	0.0486	0.0552	22.82	35.82	39.31	1.4457	2.3343	0.0982	1.0000
2.28	0.0486	0.1110	22.57	46.40	32.88	1.1160	5.6123	0.0528	1.0000
11.36	0.0486	0.5520	22.03	65.99	69.53	0.7846	13.1991	0.0000	1.0000
$Ca = 1 \times 10^{-6}$ [e]									
0.12	0.0852	0.0105	56.14	13.99	17.11	6.4897	1.0201	0.2263	0.9957
0.49	0.0852	0.0420	41.03	20.21	24.80	4.4921	2.8151	1.0000	1.0000
1.23	0.0852	0.1050	31.81	34.68	44.03	2.6178	3.9647	0.5302	0.5995
2.47	0.0852	0.2100	29.87	59.01	76.73	1.5383	4.5501	0.3702	0.2893
12.96	0.0852	1.1040	15.55	92.68	112.32	0.9794	16.3406	0.7752	0.2256
$Ca = 5 \times 10^{-6}$ [f]									
0.09	0.4860	0.0420	57.43	32.02	29.33	16.170	2.3803	0.9972	0.8355
0.57	0.4860	0.2760	55.28	47.36	39.41	10.933	11.642	0.8423	0.8732
1.14	0.4860	0.5520	38.46	69.35	55.58	7.4660	16.511	0.1308	0.8336
2.27	0.4860	1.1040	22.19	82.00	81.79	6.3146	22.440	1.0000	0.0000

[a] $Ca = 5.23 \times 10^{-7}$. [b] $Ca = 9.84 \times 10^{-7}$. [c] $Ca = 5.23 \times 10^{-6}$. [d] $Ca = 5.79 \times 10^{-7}$. [e] $Ca = 1.01 \times 10^{-6}$. [f] $Ca = 5.79 \times 10^{-6}$.

$$k_{ri} = k_{ri}(S_1, Ca, r, \kappa, \cos\theta_e) \tag{3}$$

and

$$k_{rij} = k_{rij}(S_1, Ca, r, \kappa, \cos\theta_e) \tag{4}$$

where the subscripts i and j take the values 1 and 2 for water and oil, respectively.

Even though eqs 2 and 4 (or the simpler version of eqs 1 and 3) do not constitute a proper Onsager-type theoretical model, they are, nevertheless, "pressed into service" in all kinds of calculations of 2φFPM, including displacement flows that involve steep saturation gradients. To this end, however, the dependence of the relative permeability coefficients (conventional or traditional) on the local flow rates is usually neglected completely. The consequences of this practice on the reliability of the predicted results have still to be investigated carefully and systematically. A first step in this direction was made,[20] where the effects of the local capillary number on the relative permeabilities and the capillary pressure versus saturation relationship were taken into account explicitly.

Apart from the issue that the effects of the local capillary number cannot be neglected in displacement flows, the debate as to whether eqs 2 and 4 constitute a better model than eqs 1 and 3 is still undecided for the general case. However, the latter issue has been resolved for the relatively simple case of SSFD2φFPM, for which it has been shown that the two formulations are essentially equivalent.[4] The argument for this is as follows. If we combine the two formulations, we obtain

$$k_{ri} = k_{rii} + \frac{\mu_i}{\mu_j} k_{rij} \frac{\Delta P_j}{\Delta P_i}, \quad i, j = 1, 2, \quad i \neq j \tag{5}$$

In this equation the first term on the right-hand side is the part of the conventional relative permeability to fluid i that can be attributed to the effect of the pressure gradient in the same fluid, whereas the second term is the part that is caused through viscous coupling with the other moving fluid.

Introducing the concept of coupling indices, which are defined by

$$\chi_i = 1 - \frac{k_{rii}}{k_{ri}}, \quad i = 1, 2 \tag{6}$$

and using eqs 5 and 6 we obtain

$$\chi_i = \frac{\mu_i}{\mu_j} \frac{k_{rij}}{k_{ri}} \left(\frac{\Delta P_j}{\Delta P_i} \right), \quad i, j = 1, 2, \quad i \neq j \tag{7}$$

Close examination of the experimental data suggests a further simplification. In all cases (namely, those reported for intermediate wettability[4] and the present work), it was found that under fully developed steady-state conditions the pressure gradients in the two fluids were identical. According to this observation, eqs 5−7 can be simplified as

$$k^o_{ri} = k^o_{rii} + \frac{\mu_i}{\mu_j} k^o_{rij}, \quad i, j = 1, 2, \quad i \neq j \tag{8}$$

and

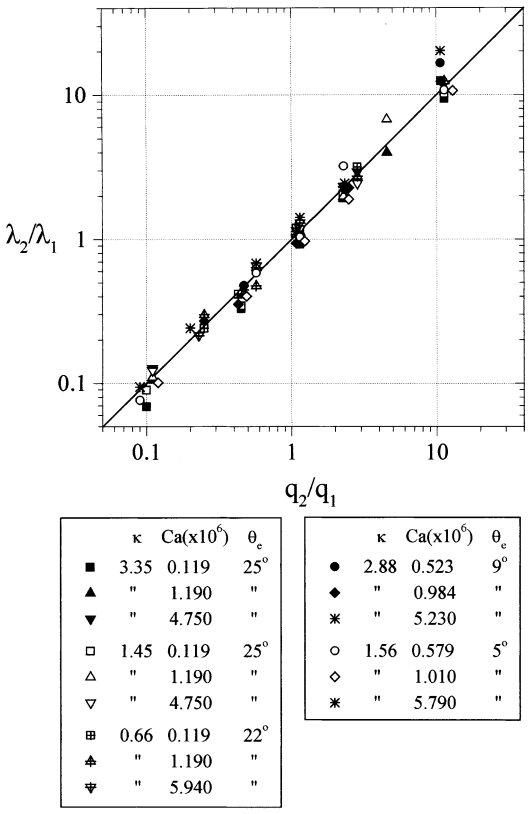

Figure 1. Plot of the mobility ratio, λ_2/λ_1, versus flow rate ratio, q_2/q_1.

$$\chi^o_i \equiv 1 - \frac{k^o_{rii}}{k^o_{ri}} = \frac{\mu_i}{\mu_j} \frac{k^o_{rij}}{k^o_{ri}}, \quad i, j = 1, 2, \quad i \neq j \tag{9}$$

where the superscript o denotes fully developed steady-state conditions, i.e., absence of boundary and end effects.

Of course, fully developed conditions constitute an ideal situation. In practice, a ratio of pressure drops that is close to unity is to be considered as direct evidence that boundary and end effects have been successfully reduced. This important experimental finding can be presented in a way that provides additional physical insight. Dividing the two components of eq 1, one obtains

$$\frac{\lambda_2}{\lambda_1} \equiv \frac{k_{r2}/\mu_2}{k_{r1}/\mu_1} = \frac{q_2}{q_1} \frac{\Delta P_1}{\Delta P_2} \tag{10}$$

where $\lambda_i \equiv k_{ri}/\mu_i$ ($i = 1, 2$) are the mobilities of the two fluids. However, if one assumes that $\Delta P_1 = \Delta P_2$, as is expected for SS2φFDFPM, eq 10 becomes

$$\frac{\lambda_2}{\lambda_1} \equiv \frac{k_{r2}/\mu_2}{k_{r1}/\mu_1} = \frac{q_2}{q_1} \equiv r \tag{11}$$

A good test of whether the relation $\Delta P_1 = \Delta P_2$ holds is to make a plot of λ_2/λ_1 versus $q_2/q_1 = r$ values and check whether the data points group along the diagonal. This is done in Figure 1, using the intermediate wettability data[3] along with the strong wettability data of the present work (Table 3). As it turns out, the result $\Delta P_1 = \Delta P_2$ is strongly confirmed.

The raw data for the case of strong wettability are summarized in Table 3, along with the corresponding

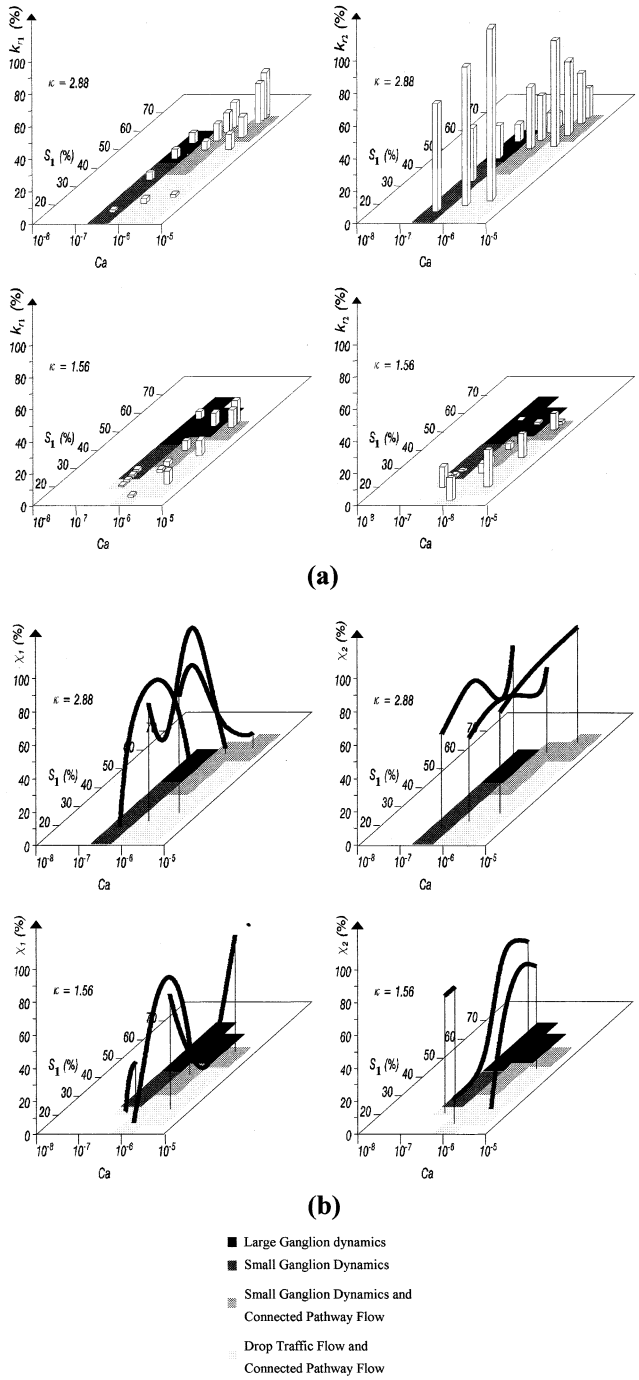

Figure 2. (a) Map of flow regimes and conventional relative permeabilities in the domain of parameters Ca, S_1, κ, for the case of strong wettability. (b) Map of flow regimes and coupling indices in the domain of parameters Ca, S_1, and κ, for the case of strong wettability.

relative permeabilities and coupling indices. The method that was used to derive the conventional relative permeabilities was the same as that used previously,[3] and it is straightforward. The method used to derive the generalized relative permeabilities was the same as that also used previously[4] and involves a global parameter estimation technique. The values of the coupling indices were obtained from eq 7, once the conventional and generalized relative permeability coefficients had been determined.

Figure 2 shows the conventional relative permeabilities and the coupling indices in the domain of parameters S_1, Ca, and κ, for the case of strong wettability. The correlation of the relative permeabilities and the coupling indices with the corresponding flow regimes is also shown.

5. Discussion

The experimental work presented here concerns the microscopic mechanisms of steady-state two-phase flow in porous media and their manifestation at the macroscopic scale. It also concerns the way in which the various flow regimes are developed as the flow parameters gradually change and their correlation with the macroscopic transport coefficients. Furthermore, it offers a quantitative description of SSFD2φFPM by means of either the conventional or the generalized relative permeability coefficients, but it also shows that neither of these theoretical formulations is truly suitable for this class of flows. Even though it is always possible to obtain and use quantitative information in the form of relative permeabilities, conventional or generalized, these do not fit in any linear macroscopic theory of the Onsager type. The explanation for this type of behavior becomes clear when one considers the many irreversible pore-scale flow phenomena, which are collectively called ganglion dynamics (mobilization, stranding, breakup, coalescence, etc.). This implies that microscopic reversibility does not hold and that new theoretical models should be developed which will take into account the true mechanisms of the flow. Such a first step has been reported.[21]

In summary, in the case of strong wettability and for small values of Ca, the oil flows mainly in the form of ganglia and droplets, whereas the water maintains its connectivity. Only at higher values of the capillary number ($Ca > \sim 5 \times 10^{-6} - 1 \times 10^{-5}$) are continuous oil pathways created connecting the fluid inlet and outlet. Still, oil ganglia or droplets flow between the oil pathways. In every case, the disconnected parts of the oil seem to contribute substantially or even totally to the flow of oil.

Motion of oil ganglia is observed over the entire range of values of the flow parameters (Ca, r, κ, θ_e) investigated here, because mobilization of the ganglia can happen even at very low values of Ca. According to the ganglion mobilization criterion[3,22,23] the real driving force necessary to overcome the resistance to ganglion motion, which is exerted by the capillary forces, depends on the shape of the oil ganglia, their orientation with respect to the macroscopic flow direction, the local pore geometry and topology, and, most importantly, on the local pressure gradient. The ratio of the driving viscous forces over the resisting capillary forces forms the pertinent dimensionless parameter for oil ganglion mobilization,[22] i.e., the ganglion mobilization number, Gm, and not the capillary number, Ca, as is usually assumed. Gm is inversely proportional to the water relative permeability, and at high oil saturation (when the water relative permeability is low), it can take values much higher than unity irrespective of the value of Ca (even at very low Ca values). For these reasons, ganglion dynamics is observed in all of the observed flow regimes.

As the values of Ca and r increase, the mean size of the ganglia decreases, until eventually oil droplets are formed with diameters comparable to those of the throats. For even larger values of Ca and r, continuous oil pathways appear along with ganglion dynamics and/or drop traffic flow that take place between the connected oil pathways.

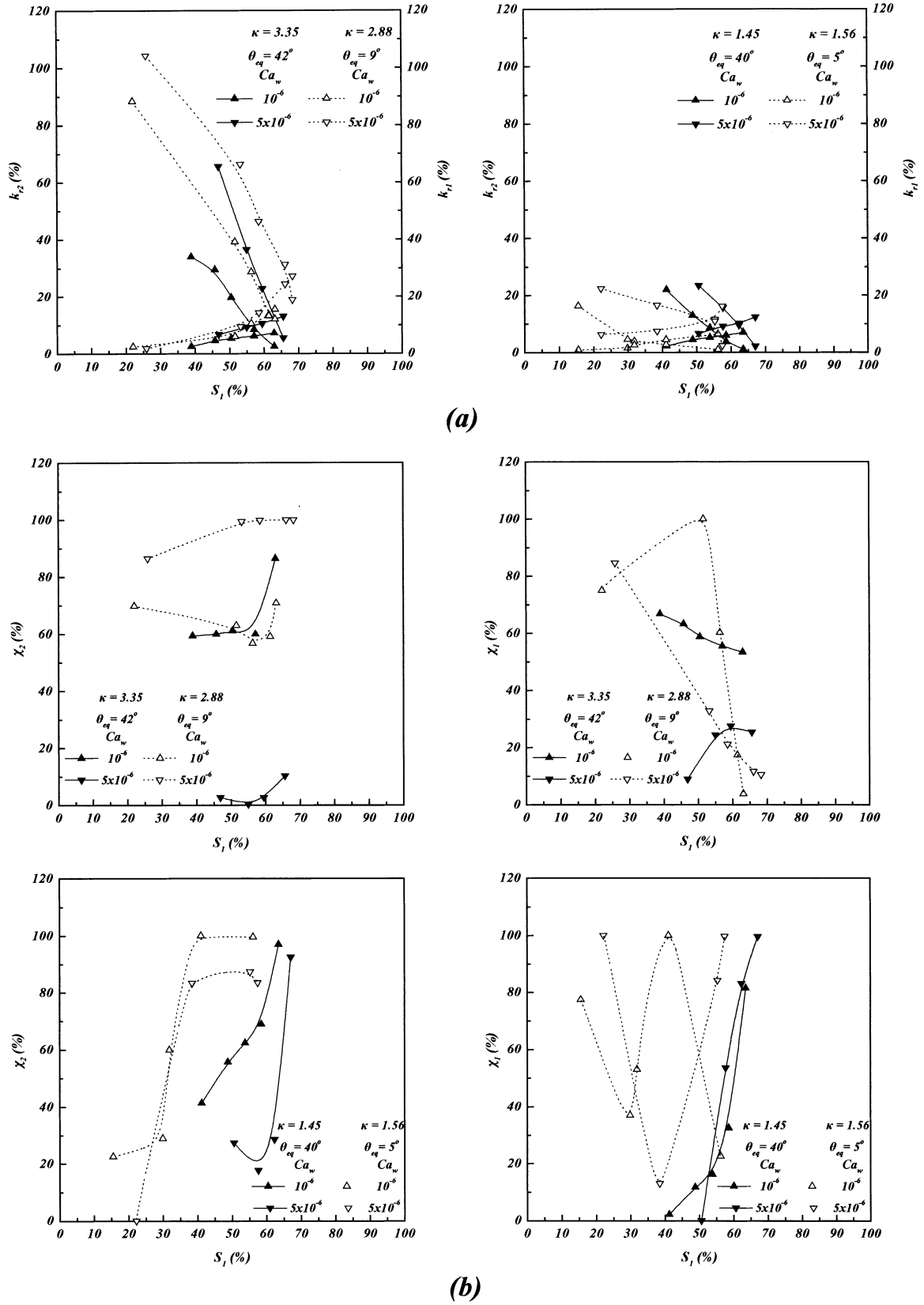

Figure 3. (a) Comparison of fluid conventional relative permeabilities for intermediate and strong wettability conditions. (b) Comparison of viscous coupling indices for intermediate and strong wettability conditions.

The gradual changes of the flow regimes are shown in Figure 2 in terms of the parameters (Ca, S_1, κ) for the case of strong wettability. All other parameters are kept constant. It should be noted that qualitatively similar results were obtained in the case of indermediate wettability.[3] The change of the wettability, from intermediate to strong, causes a broadening of the areas of small ganglion dynamics and drop traffic flow. This broadening is more intense for the larger viscosity ratio ($\kappa = 2.88$). Accordingly, the conventional relative permeabilities become larger at the same saturation level; the relative permeability to oil increases to a larger

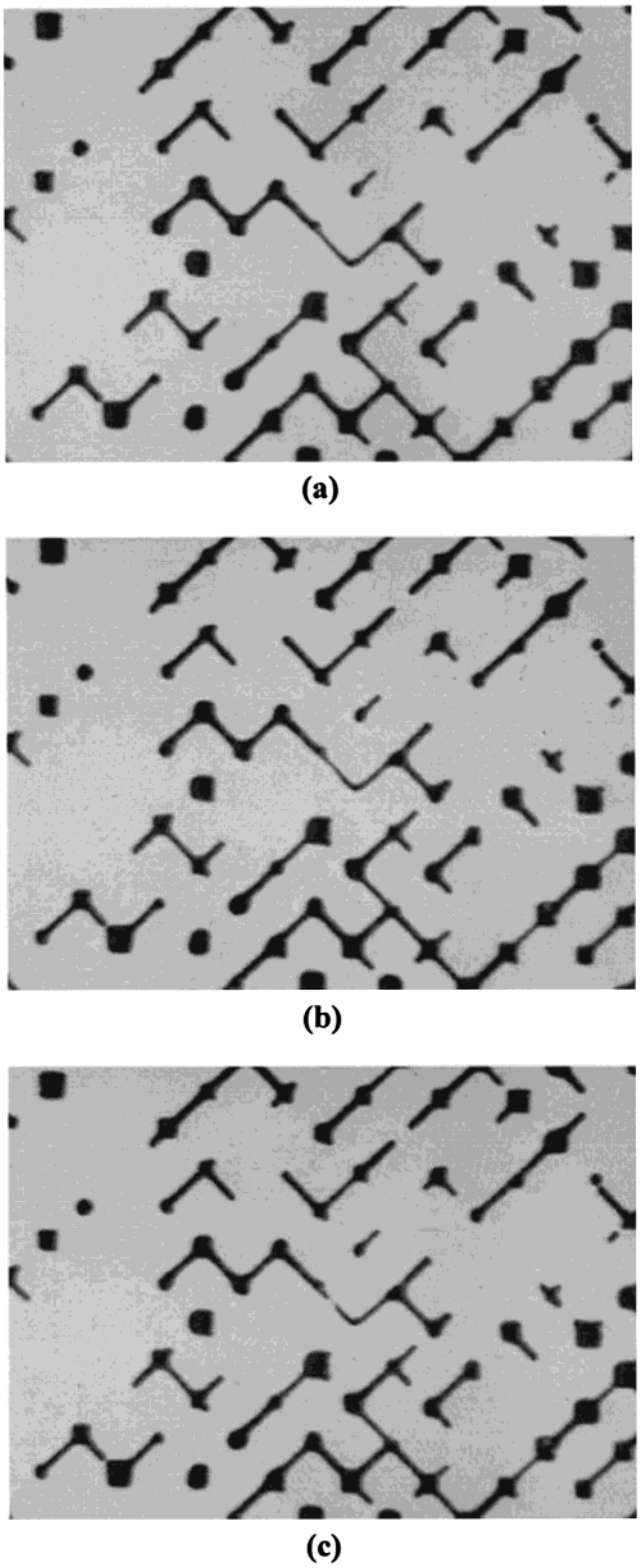

Figure 4. Successive snapshots of pinch-off in a throat ($Ca = 5 \times 10^{-7}$, $r = 1.16$, $\kappa = 2.88$).

extent than that of the relative permeability to water. This, however, does not imply that high wettability favors oil displacement. Actually, during imbibition flows, high wettability causes excessive oil disconnection through the action of wetting films, leading to higher oil entrapment.[19,24] In Figure 3a, the fluid relative permeabilities obtained in the case of intermediate wettability conditions are compared to those obtained in the case of strong wettability conditions.

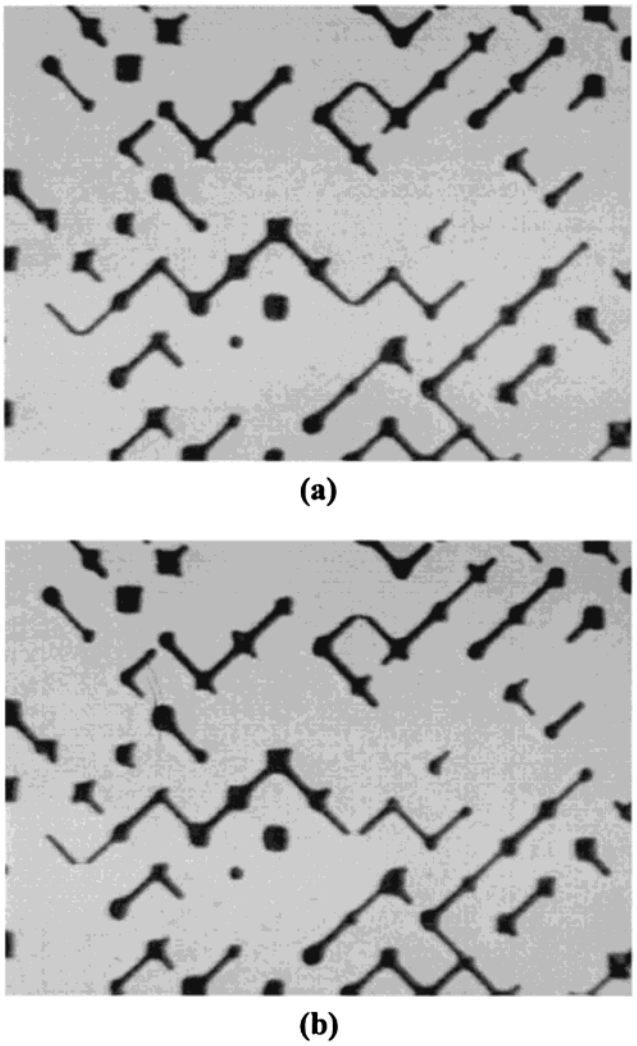

Figure 5. Successive snapshots of pinch-off in a chamber ($Ca = 5 \times 10^{-6}$, $r = 1.07$, $\kappa = 2.88$).

At the pore scale, strong wettability causes more frequent breakup through pinch-off of oil threads by the wetting films in the throats. The effect of wetting films in throats is enhanced for small values of Ca and leads to the formation of more numerous small ganglia and droplets. In Figure 4 three successive snapshots of pinch-off in a throat are presented for $Ca = 5 \times 10^{-7}$. At higher values of the capillary number, rupture of oil in chambers (pinch-off in chambers) or at the junction of chambers and throats (snap-off) becomes the dominant breakup mechanism. In Figure 5 two snapshots of pinch-off in a chamber, one before and the other after the rupture of the oil thread, are presented for $Ca = 5 \times 10^{-6}$.

Strong wettability and large viscosity ratio favor the formation of smaller ganglia, oil droplets, and connected pathways over broader ranges of the system parameters. In these flow regimes the relative permeability to oil increases significantly, while the relative permeability to water also increases, but less so.

The behavior of the flow indices is more complex in the case of strong wettability than in the case of intermediate wettability.[3] To begin with, it is clear that a reciprocal Onsager-type relation does not hold. The coupling index of water, χ_1, shows a maximum when the flow regime is SGD or SGD and CPF. This is an indication that the motion of a dense population of small

ganglia assists the flow of water. On the other hand, the motion of large but sparse oil ganglia does not affect the flow of water very much. The same is true when the flow regime is CPF.

In Figure 3b, the fluid coupling indices obtained in the case of intermediate wettability conditions are compared to those obtained in the case of strong wettability conditions. When the viscosity ratio is $\kappa = 1.56$, the coupling index of oil, χ_2, has the same behavior as that in the case of intermediate wettability.[3] It is an increasing function of water saturation and takes the highest values when the flow regime is LGD, whereas it decreases significantly when the flow regime is CPF. This is a strong evidence that the mobilization of large and sparse oil ganglia is mainly caused by the flow of water. When $\kappa = 2.88$, the oil coupling index shows a local minimum as the flow regime changes from LGD to SGD and a local maximum as the flow regime changes from SGD to DTF or from SGD to CPF (CPF and SGD or CPF and DTF). The oil coupling index decreases as oil ganglia become smaller, increases when oil droplets are formed, and decreases again as connected oil pathways are formed. In addition, the wetting film lubricates the motion of large oil ganglia and small oil droplets and the coupling index increases even further under such conditions, whereas it plays a minor role when the flow regime is SGD or CPF.

6. Conclusions

During steady-state fully developed two-phase flow in porous media (SSFD2φFPM) with strong wettability conditions, the oil becomes disconnected (to a large extent or even completely) in the form of ganglia and droplets. The water preserves its connectivity. This behavior is qualitatively similar to that observed in the case of intermediate wettability.

The formation of wetting films in the case of strong wettability is a dominant factor. It promotes the disconnection of oil, but it also lubricates the flow of ganglia and droplets.

For small Ca values ($Ca < \sim 10^{-6}$) the flow of oil takes place through the motion of ganglia and/or droplets. For large values of the capillary number ($Ca \geq \sim 10^{-6}$) connected pathways for the flow of oil are formed, but the motion of ganglia and droplets between connected oil pathways persists and contributes significantly to the oil flow rate.

The flow rates of the fluids are nonlinear functions of the pressure gradients. The conventional as well as the generalized relative permeabilities depend strongly not only on saturation but also on capillary number, Ca, flow rate ratio, r, viscosity ratio, κ, and wettability.

Strong wettability conditions and large viscosity ratio produce cooperative effects that cause increases of the relative permeability to both fluids at any given saturation value. They also increase oil saturation, when all other parameters are kept constant.

The coupling indices are complex functions of the system parameters and are correlated with the pore-scale flow mechanisms. An Onsager reciprocal relation does not hold, because the flow involves many nonlinear irreversible microscopic phenomena that cause microscopic irreversibility.

Nomenclature

A = cross-sectional area of the model porous medium
Ca = capillary number = $\mu_1 q_1/\gamma_{12} A$
k = absolute permeability
k_{ri} = conventional relative permeability to fluid i
k_{ri}^o = value of k_{ri} free from boundary and end effects
k_{rij} = generalized relative permeability coefficients
k_{rij}^o = value of k_{rij} free from boundary and end effects
L = distance along which ΔP_1 and ΔP_2 are measured
$r = q_2/q_1$ = flow rate ratio
q_i = flow rate of fluid i
S_i = saturation of fluid i

Greek Symbols
γ_{12} = interfacial tension
Δp_i = pressure drop (negative) in fluid i
θ_e = equilibrium contact angle
$\kappa = \mu_2/\mu_1$ = viscosity ratio
$\lambda_i = k_{ri}/\mu_i$ = mobility of fluid i
μ_i = viscosity of fluid i
ρ_i = density of fluid i
χ_i = coupling index of fluid i
χ_i^o = value of χ_i free from boundary and end effects

Subscripts
i = fluid index
1 = water
2 = oil

Superscript
o = free from boundary and end effects

Literature Cited

(1) Rose, W. Richards' Assumptions and Hassler's Presumptions. *TiPM* **1991**, *6*, 91.

(2) Honarpur, M.; Mahmood, S. M. Relative-Permeability Measurements: An Overview. *J. Pet. Technol*. **1988**, Aug, 963.

(3) Avraam, D. G.; Payatakes, A. C. Flow Regimes and Relative Permeabilities during Steady-State Two-Phase in Porous Media. *J. Fluid Mech*. **1995**, *293*, 207.

(4) Avraam, D. G.; Payatakes, A. C. Generalized Relative Permeability Coefficients during Steady-State Two-Phase Flow in Porous Media, and Correlation with the Flow Mechanisms. *TiPM* **1995**, *20*, 135.

(5) Avraam, D. G.; Kolonis, G. B.; Roumeliotis, T. C.; Konstantinides, G. N.; Payatakes, A. C. Steady-State Two-Phase Flow Through Planar and Nonplanar Model Porous Media. *TiPM* **1994**, *16*, 75.

(6) Tzimas, G. C.; Matsuura, T.; Avraam, D. G.; Van Der Brugghen, W.; Constantinides, G. N.; Payatakes A. C. The Combined Effect of the Viscosity Ratio and the Wettability during Forced Imbibition through Non-Planar Porous Media. *J. Colloid Interface Sci*. **1997**, *189*, 27.

(7) Sandberg, C. R.; Gournay, L. S.; Sippel, R. F. The Effect of Fluid-Flow Rate and Viscosity on Laboratory Determinations of Oil−Water Relative Permeabilities. *Trans. Am. Inst. Min., Mettal. Pet. Eng.* **1958**, *213*, 36.

(8) Lefebvre Du Prey, E. J. Factors Affecting Liquid−Liquid Relative Permeabilities of a Consolidated Porous Medium. *Soc. Pet. Eng. J*. **1973**, Feb, 39.

(9) Amaefule, J. O.; Handy, L. L. The Effects of Interfacial Tensions on Relative Oil/Water Permeabilities of Consolidated Porous Media. *Soc. Pet. Eng. J*. **1982**, June, 371.

(10) Fulcher, R. A.; Ertekin, T.; Stahl, C. D. Effect of Capillary Number and its Constinuents on Two-Phase Relative Permeability Measurements. *J. Pet. Technol*. **1985**, Feb, 249.

(11) Leverett, M. C. Capillary Behavior in Porous Solids. *Trans. Am. Inst. Min., Metall. Pet. Eng.* **1941**, *142*, 152.

(12) Geffen, T. M.; Owens, W. W.; Parrish, D. R.; Morse, R. A. Experimental Investigation of Factors Affecting Laboratory Relative Permeability Measurements. *Trans. Am. Inst. Min., Metall. Pet. Eng.* **1951**, *192*, 99.

(13) Yuster, S. T. Theoretical Considerations of Multiphase Flow in Idealized Capillary Systems. *World petroleum congress proceedings, Section II. Drilling and production*, The Hague, 1951.

(14) Odeh, A. S. Effect of Viscosity Ratio on Relative Permeability. *J. Pet. Technol*. **1959**, *11*, 346.

(15) Owens, W. W.; Archer, D. L. The Effect of Rock Wettability on Oil−Water Relative Permeability Relationships. *J. Pet. Technol.* **1971**, July, 873.

(16) McCaffery, F. G.; Bennion, D. W. The Effect of Wettability on Two-Phase Relative Permeabilities. *J. Can. Pet. Technol.* **1974**, Oct−Dec, 42.

(17) Jerault, G. R.; Salter, S. J. The Effect of Pore Structure on Hysteresis in Relative Permeability and Capillary Pressure: Pore-Level Modeling. *TiPM* **1991**, *5*, 103.

(18) Smedley G.; Coles D. Some Transparent Immiscible Liquid Pairs. *J. Colloid Interface Sci.* **1990**, *138* (1), 42.

(19) Vizika, O.; Payatakes, A. C. Parametric Experimental Study of Forced Imbibition in Porous Media. *Phys. Chem. Hydrody.* **1989**, 11, 187.

(20) Tsakiroglou, C. D.; Avraam, G. D.; Payatakes, A. C. Improved Macroscopic Equations of Two-Phase Flow in Porous Media Based on New Models of the Capillary Pressure and Relative Permeability. *Proceedings of the XII International Conference on Computational Methods in Water Resources*, Crete, Greece, June 15−19, 1998.

(21) Valavanides, M. S.; Constantinides, G. N.; Payatakes, A. C. Mechanistic Model of Steady-State Two-Phase Flow in Porous Media Based on Ganglion Dynamics. *TiPM* **1998**, *30*, 267.

(22) Ng, K. M.; Payatakes, A. C. Stochastic Simulation of the Motion, Breakup and Stranding of Oil Ganglia in Water−Wet Granular Porous Media during Immiscible Displacement. *AIChE J.* **1980**, *26*, 419.

(23) Payatakes, A. C.; Dias, M. M. Immiscible Microdisplacement and Ganglion Dynamics in Porous Media. *Annu. Rev. Fluid Mech.* **1984**, *2*, 85.

(24) Vizika, O.; Avraam, D. G.; Payatakes, A. C. On the Role of Viscosity Ratio in Low Capillary Number Immiscible Microdisplacement. *J. Colloid Interface Sci.* **1994**, *165*, 386.

Received for review June 16, 1998
Revised manuscript received October 23, 1998
Accepted October 23, 1998

IE980404O